Bagheinia and Ghassemi *International Journal of Mechanical and Materials Engineering* (2018) 13:1
DOI 10.1186/s40712-017-0087-1

International Journal of Mechanical and Materials Engineering

ORIGINAL PAPER Open Access

Simulated and experimental investigation of the airfoil contour forming of 301 austenitic stainless steel considering the springback

Reza Bagheinia and Aazam Ghassemi*

Abstract

Background: Metal forming has played a significant role in manufacturing development, thus investigations in the field of metal forming to improve the quality of the forming process are necessary. In the present study, the experimental and numerical analysis of airfoil contour forming of 301 austenitic stainless steel is examined in order to reduce the spring reversible ability under preheat temperature.

Method: Considering the stress-strain properties of the preheat temperature; the body forming is simulated in ABAQUS software according to the theory of increasing the blank holder force during forming.

Results: The obtained results of the spring-back for simulating the austenitic stainless steel airfoil are compared and investigated with the manufactured experimental sample results using deep tensile forming.

Conclusions: By comparing the results it can be seen that the control of blank holder force during forming cause to minimize the spring-back effects.

Keywords: Austenitic stainless steel, Springback, Airfoil, Work hardening

Background

Nowadays, the stainless steel is one of the most usable steels in automotive, military, and airborne industries. This is due to unique features such as high corrosion resistance and good formability (Bart et al. 2013). Other features of these steels such as ease of welding, soft and flexible for cold working, and to be non-magnetic are of interest to many researchers and industrialists (Luo 2013; Haghshenas 2016). The most outstanding of these steels are the ferritic stainless steels (400 series) (Henry and Maloy 2017; Löytty et al. 2016; Zhao et al. 2016), precipitation hardening stainless steels (Couturier et al. 2016; Silvestre et al. 2015), duplex stainless steels (austenitic-ferritic) (Schwarm et al. 2017; Mukherjee and Pal 2012; Samal et al. 2011), martensitic stainless steel alloys (Wiessner et al. 2017; Garrison and Amuda 2017), and austenitic stainless steels (200 and 300 series) (Tasker and Amuda 2017; Borgioli et al. 2016). Simulation of the springback depends on two main groups of parameters: the first group is the physical parameters such as mechanical properties, hardness, and friction coefficient rules, and the second group is numerical parameters such as the number of embedded points in the thickness direction, element type, mesh size, and the convergence tolerances that further are concerned with the simulating conditions of body.

Padmanabhan et al. (2002) examined the effect of the back force applied to the workpiece on the springback. The force applied by the hydraulic ram makes more tensile strain in the body and reduces the amount of springback. They showed that the increase of the applied back force in the sample causes the springback angle to reduce. Kuwabara et al. (2009) investigated the effect of the rolled direction on the springback. They evaluated the springback angle of the various steels with the different yield stress and found that the effect of springback in the tangential direction of rolling always is less than

* Correspondence: aazam77@yahoo.com; a_ghassemi@pmc.iaun.ac.ir
Department of Mechanical Engineering, Najafabad Branch, Islamic Azad University, Najafabad, Iran

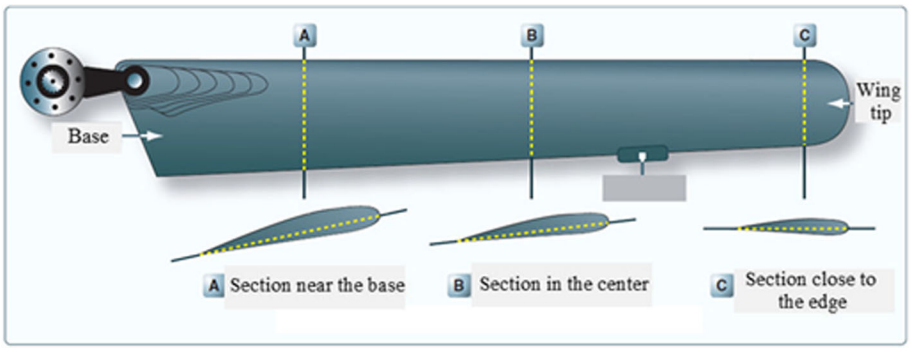

Fig. 1 The helicopter fin (Federal Aviation Administration 2014)

the perpendicular direction. Zhang et al. (2010) invented the multi-step compensation method to modify the springback direction. In this method, the die surface shape is compared with the actual piece based on the results of the simulation. After the first applied modification of the die, the die surface is simulated again and the results are compared with the actual piece. This is repeated until the deviation between simulation results and the actual piece is minimized. Uemori et al. (1998) studied the modeling type of the plastic hardening in the accuracy of the simulation. For this purpose, they examined the linear kinematic hardening and the combination of linear and nonlinear kinematic hardening model and it is concluded that the results of simulation in combined model is very similar to reality. The effect of simultaneous tension and pressure applied to the sheet during the forming process is investigated by Schilp et al. (2012). They studied springback factor using tensile pushing-bending, and stretch-bending for two bend angles 45° and 90°. They reported that the stretch-bending case is the best state to reduce the amount of springback. Sing and Agnihotri (2015) studied the parameters affecting the formation of deep stretch. They found that the blank holder force is the most important parameter that must be selected carefully in the deep tensile forming. They revealed that the blank holder force is the only parameter that alone directly affects the outputs such as material flow, variations of the thickness, and tear and shrinkage behavior. Liu et al. (2002) tried to minimize the amount of springback using the changing of the blank holder force. After a certain time, they exerted a large blank holder force on the walls to create a large plastic strain and thereby slowed down the flow of material into the die cavity. In this way, instead of reaching the blank holder force from zero to its maximum value in a short period of time of forming, and remaining constant during the forming period, it starts from an initial value and after a determined period of time, t_1, progressively reaches to the second value and remains constant in the same amount of force up to the end of time of forming, t_t. Then, they obtained the modified model of the technique that both of the primary and the secondary blank holder force can be calculated utilizing a mathematical algorithm. Accordingly, the primary blank holder force is computed as

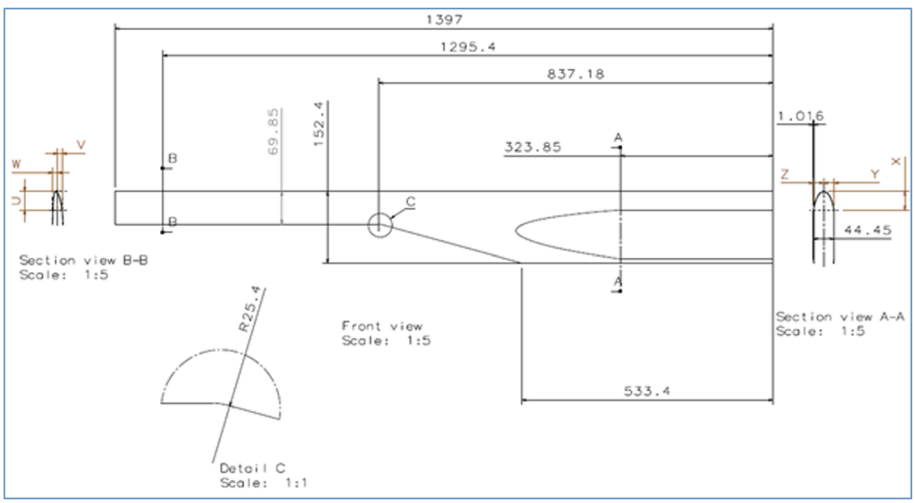

Fig. 2 Sketch of the helicopter tail rotor is designed to cover the rubbing ballet

Table 1 Geometrical characteristics of the fin tail rotor

Geometrical characteristics	Value (mm)
Total length	1397
The width of the largest outfall	44.45
The width of the smallest outfall	Variable
The height of the largest outfall	152.4
The height of the smallest outfall	69.85
Thickness	1.016
Approximate dimensions of the spreadsheet	350 × 1397
Fixed length of the largest cross section	533.4
Fixed length of the smallest cross section	101.6

the force value that causes to lock the plate between the matrix and blank, and the secondary blank force is also estimated to be the maximum blank holder force.

The paper presents the airfoil contour forming of a helicopter tail rotor with specific dimensions and material that is studied and analyzed to reduce the springback after forming and to prevent work hardening process. Then, the blank holder force is calculated based on the technique used by Liu et al. and the austenitic stainless steel of class 301 with a surface pressure of 0.163 MPa is employed. The feature of this kind of steel, the high springback after the forming process, and work hardening during forming can be mentioned so that the forming during the process is faced with the problems in conventional methods of forming. On the other hand, the very low thickness of the steel sheet can be noted that causes forming the deep drawing process require very precise dimensional tolerances of the die. Another important point is that the length of the piece and very small bandwidth leads to remove many forming techniques such as explosive forming. Finally, the obtained results of experimental and numerical analysis of finite element method (FEM) are compared and evaluated. In order to prevent the strain hardening during the process, the sheet is formed under the temperature of 350 °C without importing the fine pieces into the structure-phase variations and changing its mechanical properties. Furthermore, the mechanical properties such as stress-strain required for simulating are considered based on the mechanical properties of this temperature.

Table 2 Point-to-point characteristics of the cross-section A-A

X	*Y*	*Z*
0	0	0
2.54	6.858	6.858
5.08	9.525	9.525
7.62	11.4808	11.4808
12.7	14.4018	14.4018
17.78	16.5862	16.5862
25.4	19.0754	19.0754
38.1	21.9456	21.9456
50.8	23.749	23.749
63.5	24.8412	24.8412
76.2	25.3492	25.3492
88.9	25.4254	25.4254
102.6	25.1206	25.1206
114.3	24.5364	24.5364
127	23.6728	23.6728
139.7	22.5806	22.5806
152.4	21.3106	21.3106
165.1	19.8882	19.8882

Table 3 Point-to-point characteristics of the cross-section B-B

X	*Y*	*Z*
0	− 3.7846	3.7846
2.54	− 0.3556	6.6802
5.08	1.143	7.6454
7.62	2.3114	8.2804
12.7	4.191	9.0932
17.78	5.6896	9.6266
25.4	7.4222	10.0838
38.1	9.525	10.668
50.8	10.7696	11.049
63.5	11.4046	11.4046
76.2	11.6586	11.6586
88.9	11.684	11.684
102.6	11.5316	11.5316
114.3	11.2776	11.2776
127	10.8712	10.8712
139.7	10.3886	10.3886
152.4	9.8044	9.8044
165.1	9.144	9.144

Methods

In this section, geometry and material characteristics of the helicopter tail rotor are expressed. Then, the specifications

Table 4 The mechanical properties of austenitic stainless steels of 301 at 25 °C (AK Steel Corporation 2007)

Mechanical properties	Value	Dimension
Density	8000	Kg/m^3
Poisson's ratio	0.27–0.3	–
Young's modulus	193	Gpa
Ultimate stress	515	Mpa
Yield stress	205	Mpa
Elongation	40	%
Hardness	88 (max)	HRB

Table 5 Various states of the work hardening of stainless steel 301 (AK Steel Corporation 2007)

Hardened state	Yield stress (PSI)	Tensile stress (PSI)	Elongation percent for 2 in. (as sample)	Hardness (Rockwell C)
¼ hard	75,000	125,000	25	25
½ hard	110,000	150,000	15–18	32
¾ hard	135,000	175,000	10–12	37
Full hard	140,000	185,000	8–9	41

of aerodynamic forces and operating conditions of ballet are determined. The base of determination of the material is required for the production of the ballet.

Airfoil

In this study, instead of the used conventional titanium airfoil samples as anti-wear coating fin tail of the helicopter rotor, the airfoil contour of austenitic stainless steel class 301 is considered because of its specific characteristics such as high springback due to its low thickness and work hardening during forming. The schematic of the helicopter fin and sketch of the helicopter tail rotor are shown in Figs. 1 and 2. Moreover, the geometrical characteristics of the tail rotor are presented in Table 1.

Control of springback is carried out on the most critical cross-section of the body, i.e., cross-section A-A, which has the most of R/t ratio. As shown in Fig. 1, the body section A-A is extended symmetrical to the right direction. In addition, from section B-B as asymmetrical to the left and from section A-A to section B-B, the body is extended as fixed asymmetric. It should be noted that the airfoil contour in both positions are point-to-point and the profile of both the positions are given in Tables 2 and 3. The airfoil motion through the air causes to create the relative airflow, which is parallel but in the opposite direction to the airfoil.

The fin warp

Since the lift force due to circulating wind flow is different around the fin, the warp must be considered for the fin firstly to minimize the stress applied to the fin and secondly to distribute the lift force over the surface, uniformly (Fig. 1). The pitch angle (the angle between the chord line and horizontal line) is the most value at closest to the rotor mast, which the fin has a lowest linear velocity, and it is lowest value at the farthest point to the fin that has a highest linear velocity. Thus, the velocity of the forced air and applied loads to the center of the rotor mast, reaches to the minimum value (Federal Aviation Administration 2014).

The fin material

The fin material should be selected such that the aerodynamic loads are tolerated by the fin. Furthermore, the elasticity of the fins must be such that the fin has the ability to carry the alternating and cyclic loads. Corrosion is one of the helicopter hollowware problems, especially for the ones that are under stress, such as fins. This issue becomes more sensitive in flight conditions on the sea. In this study, the considered material for the anti-wear coating helicopter airfoil wing is the austenitic stainless steels of 301 class because of its special physical, chemical, and metallurgical features (Smith 1987). The mechanical properties of austenitic stainless steels of group 301 are given in Table 4. The mechanical properties of austenitic stainless steel of 301 during forming operations, constantly subject to change due to the work hardening process; hence, the conditions must be controlled. Therefore, the four known modes of the steel during the forming process are introduced in Table 5.

Results and discussions

In this section, based on the following procedures, the forming process results of the abrasion coating of a helicopter fin tail rotor are examined:

I. In order to recognize that the hot or cold forming is allowed for the piece, under different temperatures, the hardness and tensile tests are taken place on the various samples of austenitic stainless steel grade 301.
II. Based on the theoretical and experimental documentaries, an abrasion coating method or process for forming the fin tail rotor is considered and then, using the results of paragraph (I) and the earlier geometrical and mechanical properties listed,

Table 6 Results of the tensile test

Sample number	Metal temperature (°C)	Elongation (%)	Yield stress (Mpa)	Ultimate stress (Mpa)	Hardness (Rockwell C-HRC)
1	25	35	276	724	26–28
2	250	37	152	552	26–28
4	350	38	134	485	26–28
5	400	43	134	463	26–28

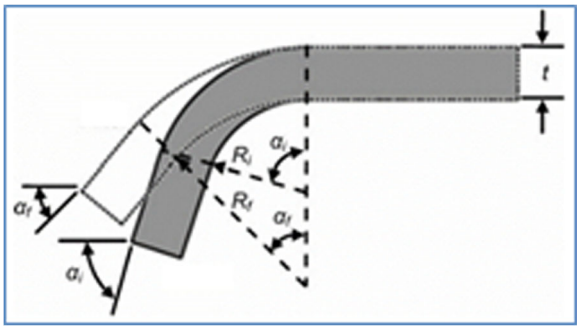

Fig. 3 Schematic of springback

the appropriate boundary conditions is utilized in the simulation.

The results of tensile and hardness test

It is expected that the amount of work hardening is increased in cold forming of the austenitic stainless steels 301 due to increase of the ultimate and yield stresses; therefore, the considered piece is formed under high-temperature conditions, here (Davis 1999). Since the steel of grade 301 becomes crystallize and its phase, and ultimately its mechanical properties are changed at temperatures above 400 °C, so the optimum temperature for hot forming must be below a temperature of 400 °C to reduce the work hardening process and thus, the mechanical properties are achieved by proper quenching the piece after forming. Accordingly, in this study, five samples of austenitic stainless steel of 301 for tensile testing are used, and besides a sample kept under ambient temperature conditions, other samples are tested in ranges between 250 and 400 °C. The test results are shown in Table 6.

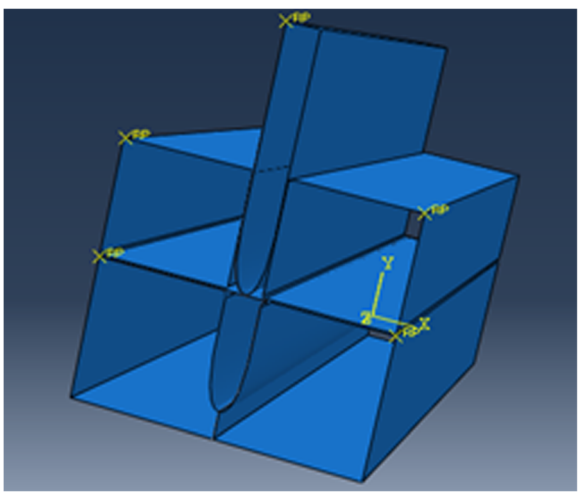

Fig. 4 The assembled pieces in ABAQUS

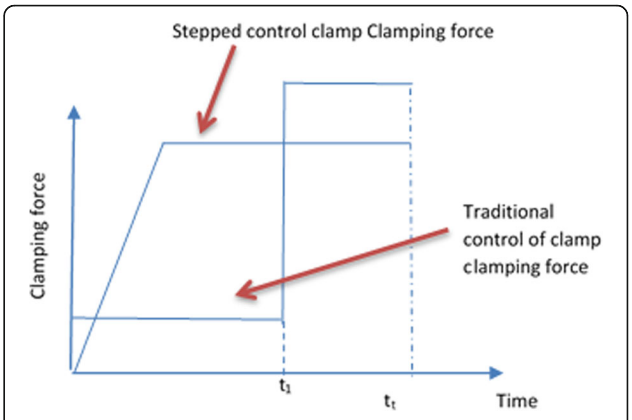

Fig. 5 Variation of blank holder force during forming

The results of Table 6 shows that before the crystallization temperature of the metal (i.e., 400 °C), the metal mechanical properties have the better conditions than the ambient temperature, while the increasing elongation percentage is also reached to stable conditions up to the crystallization temperature of the metal. Therefore, based on the obtained results of this test, it can be invoked that if the hot forming conditions of the austenitic stainless steel of 301 are provided up to the temperature of 350 °C, the destructive effects of work hardening during the process and springback after the process can be controlled. Herein, the temperature of 350 °C is considered to define the boundary conditions for practical forming and simulating the piece.

Springback control

After each plastic deformation, some plastic recovery is established. Because of the elastic band, the sheet tends to return to its previous position after coming out of the die. Then, it reaches to a balance using the plastic pressure around the body that called the springback. The permanent deformation, ε_t, is the summation of plastic deformation, ε_{pl}, and elastic deformation, ε_e, which is obtained as follows:

$$\varepsilon_t = \varepsilon_{pl} + \varepsilon_e \tag{1}$$

Until the load is applied on the piece, the body follows the dimension characteristics that appeared as a result of plastic deformation. Schematic of springback is shown in Fig. 3. Length of the bend at the neutral axis (D) is the same before and after bending, so we have (Schilp et al. 2012):

$$D = \left(R_i + \frac{t}{2}\right)\alpha_i = \left(R_f + \frac{t}{2}\right)\alpha_f \tag{2}$$

where R_i and α_i ($\alpha_i = 180 - \alpha$), respectively, are the bending radius and the bending angle before unloading, and

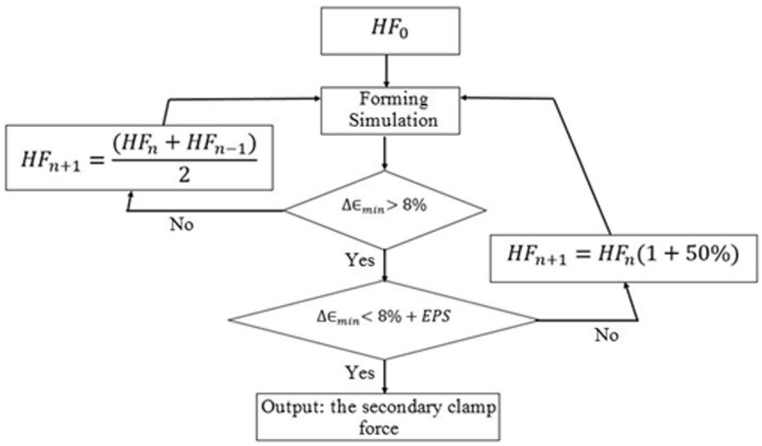

Fig. 6 Algorithm of the secondary blank holder force (Löytty et al. 2016)

R_f and α_f ($\alpha_f = 180 - \alpha$) are the bending radius and the bending angle after unloading, respectively. In addition, α is the profile angle. By introducing K_s as:

$$K_s = \frac{R_i + \frac{t}{2}}{R_f + \frac{t}{2}} = \frac{\alpha_f}{\alpha} \tag{3}$$

It can be seen that the springback factor depends only on the ratio R/t. If $K_s = 1$, there is no springback, and if $K_s = 0$, the elastic recovering is taken place completely such that the plastic deformations do not happen. The following relation is approximately established (Schilp et al. 2012):

$$\frac{R_f}{R_i} = 4\left(\frac{R_i(Y_s)}{E}\right)^3 - 3\left(\frac{R_i(Y_s)}{E}\right) + 1 \tag{4}$$

where E is Young's modulus, and Y_s is the yield stress.

To compensate the springback, the strategies such as over bending workpiece (2 to 8% more bending angle is considered), bottoming, and the bending tensile or dilation are used (Andersson 2007). It should also be noted that the effective parameters in springback and forming process under conditions of loading and unloading are the matrix geometric characteristics, plastic deformation of the workpiece, the workpiece geometry, boundary conditions, and the blank holder force (Liu et al. 2002). According to Tables 1 and 2, the R/t for the cross-section A-A ratio is higher than the cross-section B-B, so if the springback at this cross section be controlled, it could be reasoned that the springback of the whole piece have been controlled. Therefore, the simulation is considered based on the cross-section A-A and then, the springback is investigated.

Table 7 q factor for aluminum and steel

Material	q (Mpa/m^2)
Aluminum	0.8–1.2
Steel	2–2.5

The forming process simulation

In this section, based on the mechanical properties of austenitic stainless steel of 301 under temperature of 350 °C and the blank boundary conditions, the prototype die is modeled in ABAQUS software and then, the forming process is simulated.

The die and workpiece modeling

Since two parameters bending radius, R_{bending}, and thickness of the workpiece are effective for calculating the springback, and the springback amount is increased by increasing the ratio of these parameters; thus, the critical cross-section A-A is drawn in the software, and the die drawing and punch are designed on the basis of the external and internal dimensions. As shown in Fig. 4, the various parts of the sheet are assembled and the clearance size between the sheet and blank is considered equal to 0.2 mm. Moreover, the punch is intended in a tangent situation to the sheet to minimize the simulation time. Blank holder force is varied according to Fig. 5.

The purpose of the simulation is to estimate two parameters: the point of changing the blank holder force from the minimum mode to maximum, and the maximum blank holder force value in the state of transition loading.

For the sake of definition of moving phases, since the aim is to find the process locations whereby entering the punch into the matrix for a certain size, the blank holder force is ascending increased, a static phase and two explicit dynamic phases are introduced. The friction coefficient of the surfaces boundary conditions is intended equal to 0.1. According to Liu et al.'s proposed method (Padmanabhan et al. 2002), the initial pressure on the clamp is calculated using relation (5) and then,

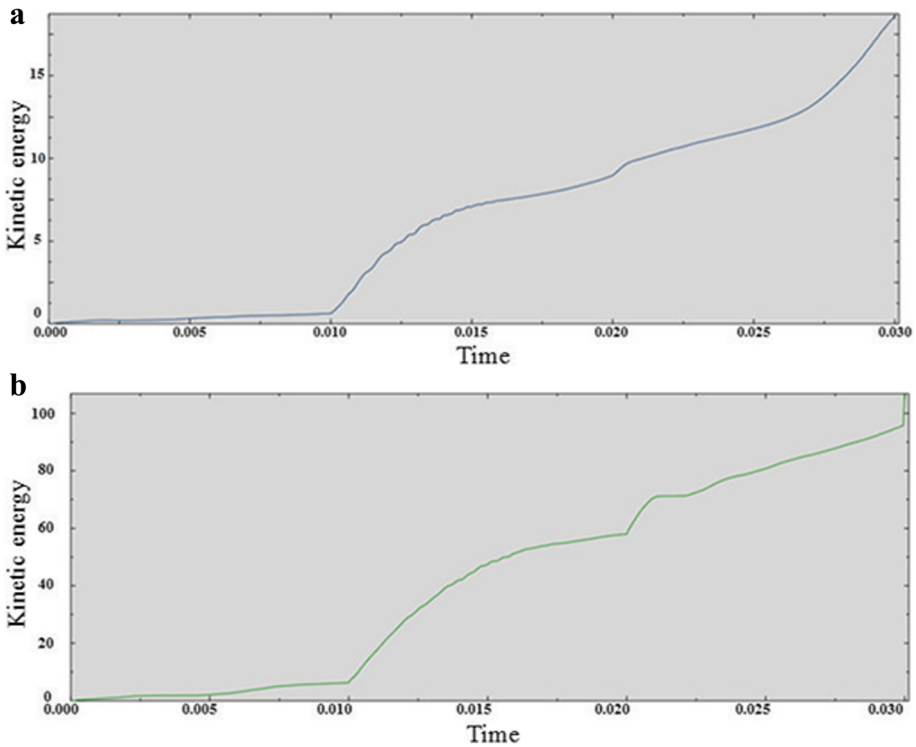

Fig. 7 **a** The kinetic energy graph of the work piece during forming and without taking into account the springback. **b** The internal energy graph during forming and regardless of the springback

the secondary force must be estimated based on the flowchart shown in Fig. 6.

$$HF_0 = Aq \tag{5}$$

In this relation, HF_0 is the first blank holder force, A is the effective area between blank and blank holder, and q is calculated from Table 7.

Blank holder force is varied according to Fig. 5.

According to relation (5), the initial pressure on the clamp is calculated equal to 0.163 (Mpa).

As mentioned before, the purpose of the simulation is to estimate two parameters: the point of changing the blank holder force from the minimum mode to maximum, and the maximum blank holder force value in the state of transition loading. In this simulation, the dimensions of the sheet mesh based on the smallest distance between two points of the sheet profile curve are considered equal to 2 mm. The results of the sheet forming analysis can be validated according to the graphs of the external work and internal energy because based on the ABAQUS given mass criteria (mass scale), the internal energy must be about five times than the kinetic energy, which it can be observed in Fig. 7.

In addition, the simulated motion at the entrance of the matrix is shown in Fig. 8a–c so that (a) shows the primary blank force loading, (b) shows the secondary blank force loading, and (c) illustrates the unloading and the appearance of the springback.

By defining the path at the entrance nodes and defining the logarithmic strain output as an intended strain criterion ($\Delta\varepsilon_{min}$) in Fig. 6, (in percentage terms), all the possible states for loading and unloading could be simulated and then, the best case for the point of change the loading from the minimum to maximum mode can be predicted.

According to the flowchart in Fig. 6, while $\Delta\varepsilon > 8\%$ and $\Delta\varepsilon < 8\% + Eps$, in order to estimate the new blank holder force pressure, its previous value should be increased by 50%. The obtained results are given in Table 8. Thus, it can be observed that the greatest amount of the pressure applied on the blank should be 1.8565 MPa (350,000 lb). Finally, the ideal boundary conditions for reaching to the least amount of springback are defined as Step1 = 30 mm, Step2 = 135 mm, P_{Step1} = 0.163 Mpa, and P_{Step2} = 1.8565 Mpa.

For estimating the transition point, it is enough that the blank holder force of this state is constant considered at 0.163 MPa (30,000 lb) for all simulating cases and the forming depth of 165 mm is divided into two defined phases. The results of this estimation are inserted in Table 9. Thus, the starting point of the force change from the minimum to the maximum value is the point where the punch is entered into the mouth of the die much as 30 mm.

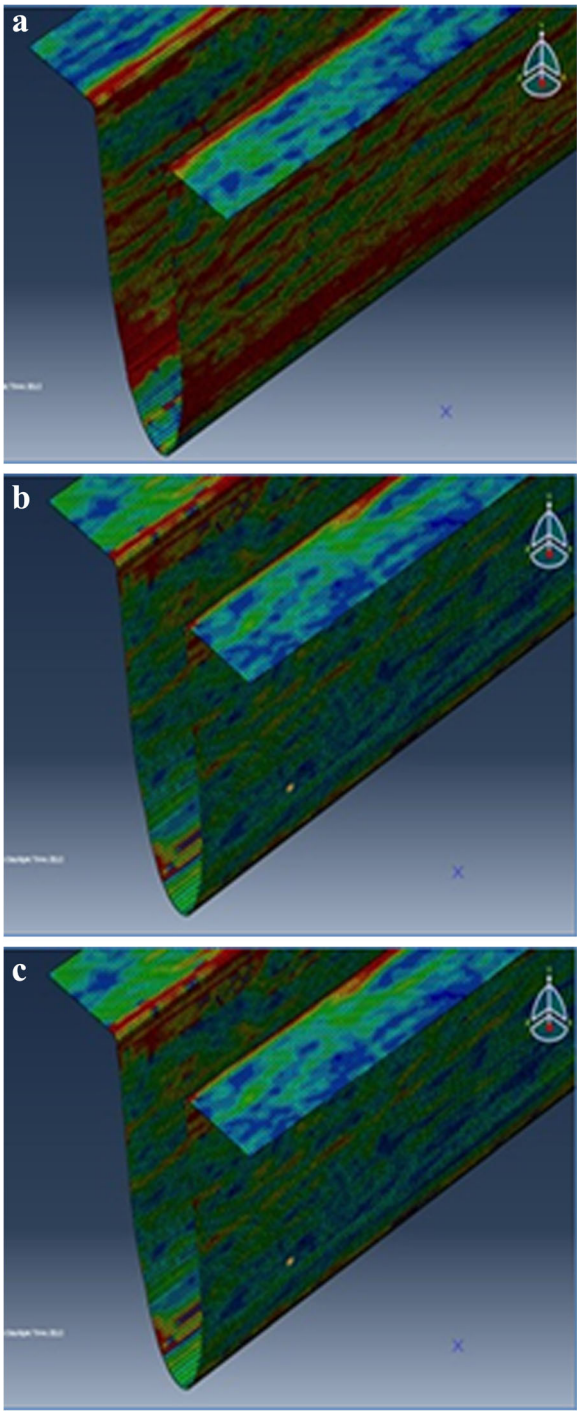

Fig. 8 a The punch loading as defined as phase 1 (static). **b** The punch loading as defined as phase 2 (explicit dynamic). **c** Unloading of the sheet

Experimental test

In this section, the piece prototype is extracted from the deep tensile die and then, the results are compared with the simulation results.

Table 8 Trial and error related to the blank pressure change between two phases and variations of the logarithmic strain

Test number	Pressure of phase 1 (Mpa)	Pressure of phase 2 (Mpa)	Logarithmic strain (%)
1	0.163	0.163	10.5753
2	0.163	0.2445	9.3986
3	0.163	0.3667	9.2097
4	0.163	0.5501	9.9174
5	0.163	0.8252	9.5038
6	0.163	1.2377	9.0166
7	0.163	1.8565	8.3665
8	0.163	2.7848	8.7862

Manufacturing the tensile forming die and extracting the sample piece

Considering the die drawing parameters of deep tensile such as the clearance between the matrix and punch and the radius of the sheet junction with the matrix mouth, the airfoil die is designed in such a way that the following conditions are satisfied:

I. The sheet is controlled along the perpendicular to the forming using the dynamic feeders.
II. When the sheet surface gets contact with the punch, the blank is involved to the sheet and the initial force is applied.
III. During moving the punch in the matrix, the sheet feeders conduct the sheet into the mouth of the channel matrix by controlling the sheet velocity, and at this stage, the blank force is reached to its maximum value.

Figures 9 and 10 display the airfoil drawn die and the designed components of the deep tensile die, respectively. As can be seen, the matrix blank is constrained in the upper shoe and the punch blank is moved up to the sheet surface using the lower shoe course and at last is bound on the sheet. The blank force is supplied by both the matrix blank and the punch blank. According to simulating process, the blank force is changed from 30,000 to 350,000 N by entering the punch in the mouth of the matrix as much as 30 mm. The feeder speed is

Table 9 Trial and error related to dividing the submergence depth between the two phases and the logarithmic strain changes

Test number	Phase 1 depth (mm)	Phase 2 depth (mm)	Logarithmic strain (%)
1	20	145	11.4907
2	30	135	10.5753
3	40	125	22.2150
4	50	115	24.3959

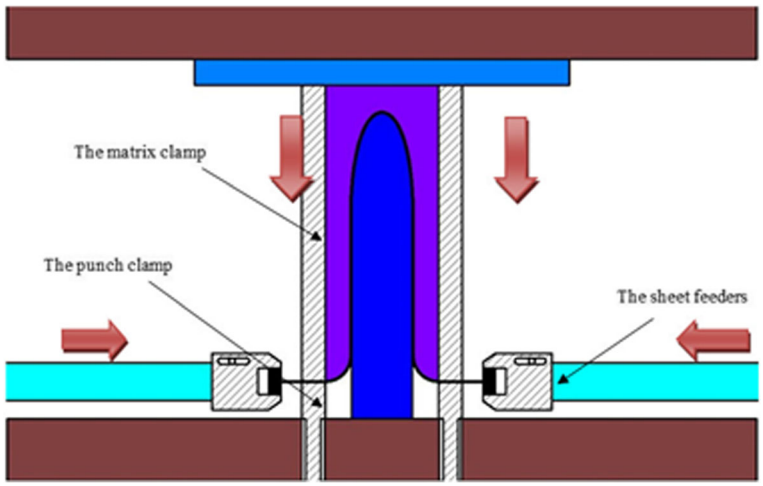

Fig. 9 The airfoil die drawing

proportional with the sheet feeding speed into the matrix. The selected hydraulic press, based on the required tonnage to apply the blank force between 30 and 350 kN, is LASCO hydraulic press machine of TZB400 model, which has a power supply 400 kN (see Fig 11). The device is equipped with a digital control unit, hydraulic cooling system, two return oil tank, and the main dynamic hydraulic unit to control the sheet flow as well as control the imposed forces on the die. In this press device, the mouth is 1000 mm and its depth is 800 mm. The deep tensile die of airfoil in hydraulic press machine is shown in Fig. 12.

Figure 13 shows the yielded sample piece. It should be noted that the piece crude metal is placed into the die with the preheat temperature of 350 °C. Next, after forming, the set of piece and die is quenched for 24 h at ambient temperature conditions and then is separated from the die. As shown in Fig. 13, in order to check the springback during the prototyping, the sheet is made to fit the sheet section contour, and it is seen that the distortion due to springback is not created in the longitudinal direction. Then, the details, related to the dimensions of the pieces measured by the coordinate measuring machine (CMM), are investigated in three coordinate directions and the obtained results are presented in Table 10. In Table 10, a column refers to the required nominal dimensions based on the piece plot and another column represents the results of experimental dimension control of the piece. Moreover, the deviation percentage of the requirement values in 17 defined points of the pieces is shown in Fig. 14. According to the results of Table 10, the maximum deviation of the measured value is about 0.9% that is acceptable for the piece because the piece to create a secondary strength is placed in another die, which the error tolerances are compensated. Therefore, the obtained results are acceptable

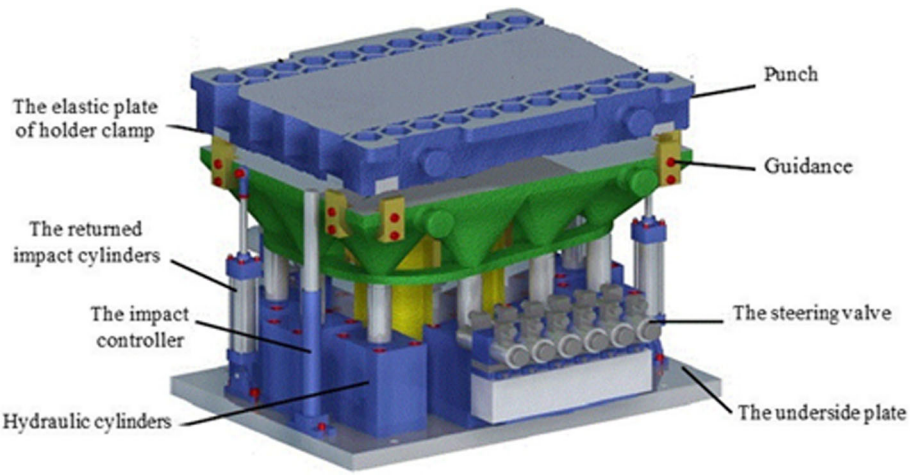

Fig. 10 Components of the airfoil deep drawing die

Fig. 11 LASCO hydraulic press machine of TZB400 model

and the piece main die can be designed. Since the simulated and tested piece section is the part of the original piece, the created piece is mounted on the tail rotor fin in order to control the situation and the status of its section is examined that it can be observed in Fig. 15.

Results

The obtained springback simulation results under the optimum boundary conditions showed that the logarithmic strain percent is approximately equal to 8% and using

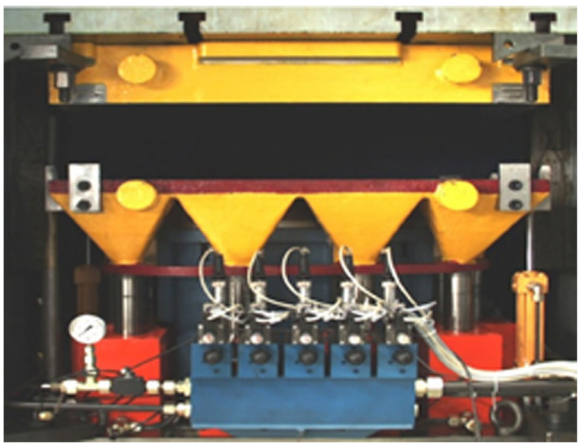

Fig. 12 The deep tensile die of airfoil in hydraulic press machine

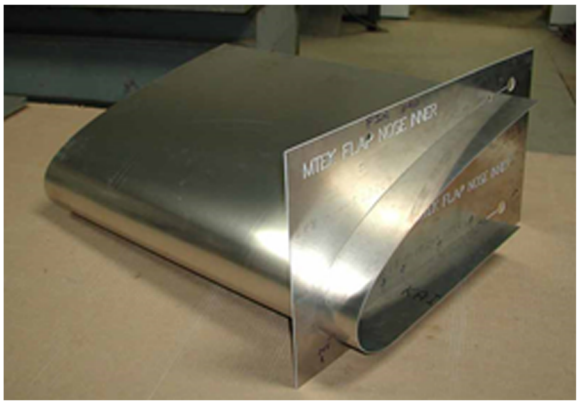

Fig. 13 The piece extracted from the tensile forming die with the length of 300 mm and depth of 165 mm

these conditions where the minimal springback is yielded, the tensile forming die is designed and manufactured. In addition, the prototype piece was achieved with a maximum deviation of 0.9% compared to the nominal value indicated in the plot. This means that the theory criterion used in this study (i.e., control of the blank force and its value) is the correct criterion and on the basis of it, the piece die can be designed and constructed in the terms of the combinational contour of symmetric-asymmetric.

Conclusions

In this study, we have tried that the forming approach of the austenitic stainless steels as well as forming the

Table 10 The deviation percentage of the measured values to the values inserted on the plot

X	Y_{main}	Y_{actual}
2.54	6.8580	6.9225
5.08	9.5250	9.5899
7.62	11.4808	11.5459
12.7	14.4018	14.4681
17.78	16.5862	16.6752
25.4	19.0754	19.1471
38.1	21.9456	22.0190
50.8	23.749	23.8243
63.5	24.8412	24.9203
76.2	25.3492	25.4291
88.9	25.4254	25.5060
101.6	25.1206	25.2025
114.3	24.5364	24.6189
127	23.6728	23.7555
139.7	22.5806	22.6637
152.4	21.3106	21.3942
165.1	19.8882	19.9723

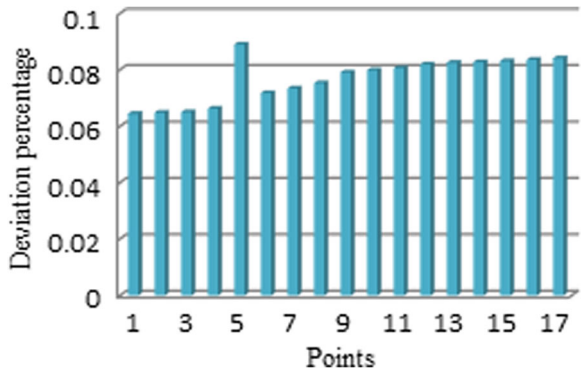

Fig. 14 The deviation percentage of the requirement values in 17 defined points of the pieces

helicopter tail rotor piece of steel grade 301 to be examined. Herein, based on the theory of Liu et al., the blank holder force is ascendant varied in during the forming. The flowchart of the secondary blank holder force is used to simulate the forming of the austenitic stainless steel sheet. In addition, to reduce the work hardening during the forming process, the initial preheat conditions were considered. Some sheet samples were placed under the various temperature conditions, and their mechanical properties were compared with the sheet tested under the ambient conditions. The result of this comparison showed that to prevent the work hardening during the process and to prevent the structure-phase changes, the preheated temperature that equal to 350 °C has closest and most optimal properties with respect to the environment temperature. The mechanical properties such as stress-strain curve required for the simulation were considered based on the abovementioned temperature. Secondly, the forming boundary condition set in such a way that when the punch goes down to 30 mm at the mouth of the die, the blank holder force is progressively shifted from the initial amount of 30,000 to 350,000 N. In order to form the intended steel group

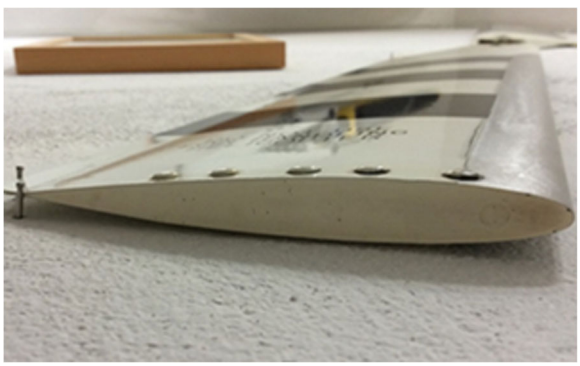

Fig. 15 Control of the assembly state of the piece with the rotor tail fin

301, the forming tensile die was designed and built based on the critical section and a sample length of 200 mm. Also, the primary and secondary blank forces are obtained using trial and error by design and construction of PLC system to control the speed of the punch relative to the velocity of movement of the plate holder jaw carriage. The hydraulic lifting jack pressure and the driver jack of the holder jaw carriage were considered based on the forming required tonnage, and then the prototype was built. Finally, by point to point controlling the resulting piece with the nominal dimensions contained in the plot, and based on the obtained results, it was concluded that the most piece deviation in the critical sections to the nominal dimensions is 0.9% that is acceptable based on the simulated logarithmic strain. Hence, it can be concluded that the piece springback has decreased. Meanwhile, by preheating the piece and cooling it under conditions of the ambient temperature, the amount of work hardening during the process is reached to its minimum value.

Author's contributions

RB performed the analysis on all samples, interpreted the data, wrote the manuscript, and acted as the corresponding author. AG supervised the development of the work, helped in the data interpretation and manuscript evaluation. Both authors read and approved the final manuscript.

Funding

No funding has been received for the conduct of this study and/or preparation of this manuscript.

Competing interests

The authors declare that they have no competing interests.

Publisher's Note

Received: 28 September 2017 Accepted: 6 December 2017
Published online: 05 January 2018

References

AK Steel Corporation, " 301 stainless steel, product data bulletin", UNS S30100, PD-134 7180–0087, 2007.

Andersson, A (2007). *Numerical and experimental evaluation of Springback in advanced high strength steel*, (pp. 301–307).

Bart, JCJ, Gucciardi, E, Cavallaro, S. (2013). 12–Biolubricant product groups and technological applications. *Biolubricants*, 565–711.

Borgioli, F, Galvanetto, E, Bacci, T. (2016). Low temperature nitriding of AISI 300 and 200 series austenitic stainless steels. *Vacuum*, *127*, 51–60.

Couturier, L, De Geuser, F, Descoins, M, Deschamps, A. (2016). Evolution of the microstructure of a 15-5PH martensitic stainless steel during precipitation hardening heat treatment. *Materials & Design*, *107*, 416–425.

Davis, JR "Stainless steels", ASM International, Day 11, 1372 AP–Technology & Engineering, Third Printing, 1999.

Federal Aviation Administration. "Helicopter Flying Handbook", Chapter 02: Aerodynamics of Flight, May 2014.

Garrison W.M, Jr., M.O.H. Amuda, Stainless Steels: Martensitic, Reference Module in Materials Science and Materials Engineering, 2017, https://doi.org/10.1016/B978-0-12-803581-8.02527-3.

Haghshenas, M. (2016). Metal–matrix composites. *Reference Module in Materials Science and Materials Engineering* https://doi.org/10.1016/B978-0-12-803581-8.03950-3.

Henry, J, & Maloy, SA. (2017). 9-Irradiation-resistant ferritic and martensitic steels as core materials for generation IV nuclear reactors. *Structural Materials for Generation IV Nuclear Reactors*, 329–355.
Kuwabara, T, Saito, R, Hirano, T, Oohashi, N. (2009). Difference in tensile and compressive flow stresses in austenitic stainless steel alloys and its effect on springback behavior. *International Journal of Material Forming*, *2*(1), 499–502.
Liu, G, Lin, Z, Bao, Y, Cao, J. (2002). Eliminating springback error in U-shaped part forming by variable blankholder force. *JMEPEG*, *11*, 64–70.
Löytty, HA, Hannula, M, Honkanen, M, Östman, K, Lahtonen, K, Valden, M. (2016). Grain orientation dependent Nb–Ti microalloying mediated surface segregation on ferritic stainless steel. *Corrosion Science*, *112*, 204–213.
Luo, AA. (2013). Magnesium casting technology for structural applications. *Journal of Magnesium and Alloys*, *1*(1), 2–22.
Mukherjee, M, & Pal, TK. (2012). Influence of heat input on martensite formation and impact property of ferritic-austenitic dissimilar weld metals. *Journal of Materials Science & Technology*, *28*(4), 343–352.
Padmanabhan, R, Sung, J, Lim, H, Oliveira, MC, Menezes, LF, Wagoner, RH. (2002). Eliminating springback error in U-shaped part forming by variable blankholder force. *JMEPEG*, *11*, 64–70.
Samal, MK, Seidenfuss, M, Roos, E, Balani, K. (2011). Investigation of failure behavior of ferritic–austenitic type of dissimilar steel welded joints. *Engineering Failure Analysis*, *18*(3), 999–1008.
Schilp, H, Suh, J, Hoffmann, H (2012). *Reduction of springback using simultaneous stretch-bending processes*, (pp. 175–180).
Schwarm, SC, Kolli, RP, Aydogan, E, Mburu, S, Ankem, S. (2017). Characterization of phase properties and deformation in ferritic-austenitic duplex stainless steels by nanoindentation and finite element method. *Materials Science and Engineering: A*, *680*, 359–367.
Silvestre, E, Mendiguren, J, Galdos, L, de Argandoña, ES. (2015). Comparison of the hardening behaviour of different steel families: from mild and stainless steel to advanced high strength steels. *International Journal of Mechanical Sciences*, *101*, 10–20.
Ch.P. Sing, G. (2015). Agnihotri, Study of deep drawing process parameters: a review, I*nternational Journal of Scientific and Research Publications, 5*(2), 1–15. ISSN 2250–3153.
Smith W. F. (1987). "Structure and properties of engineering materials", McGraw-Hill, NewYork.
Tasker, J, & Amuda, MOH. (2017). Austenitic steels: non-stainless. *Reference Module in Materials Science and Materials Engineering* https://doi.org/10.1016/B978-0-12-803581-8.09206-7.
Uemori, T, Okada, T, Yoshida, F. (1998). Simulation of springback in V-bending process by elasto-plastic finite element method with consideration of Bauschinger effect. *Metals and Materials*, *4*(3), 311–314.
Wiessner, M, Gamsjäger, E, Zwaag, SV, Angerer, P. (2017). Effect of reverted austenite on tensile and impact strength in a martensitic stainless steel—an in-situ X-ray diffraction study. *Materials Science and Engineering: A*, *682*, 117–125.
Zhang, XK, Zheng, GJ, Hu, JN, Li, CG, Hu, P. (2010). Compensation factor method for modeling springback of auto parts constructed with high-strength steel. *International Journal of Automotive Technology*, *11*(5), 721–727.
Zhao, O, Gardner, L, Young, B. (2016). Buckling of ferritic stainless steel members under combined axial compression and bending. *Journal of Constructional Steel Research*, *117*, 35–48.